Weierstraß-Institut
für Angewandte Analysis und Stochastik

Leibniz-Institut im Forschungsverbund Berlin e. V.

Preprint ISSN 2198-5855

Surface induced phase separation of a swelling hydrogel

Matthew G. Hennessy[1], Andreas Münch[1],

Barbara Wagner[2]

submitted: December 19, 2018

[1] Mathematical Institute
Andrew Wiles Building, Woodstock Road
Oxford, OX2 6GG
UK
E-Mail: hennessy@maths.ox.ac.uk
muench@maths.ox.ac.uk

[2] Weierstrass Institute
Mohrenstr. 39
10117 Berlin
Germany
E-Mail: barbara.wagner@wias-berlin.de

No. 2562
Berlin 2018

2010 *Mathematics Subject Classification.* 74H10, 82C26.

2010 *Physics and Astronomy Classification Scheme.* 83.80.Rs, 83.10.Tv.

Key words and phrases. Hydrogel, asymptotic analysis, nonlinear elasticity, phase transition.

MGH would like to acknowledge financial support from the Hooke Research Fellowship of the University of Oxford and the Marie Sklodowska-Curie Individual Fellowship.

Edited by
Weierstraß-Institut für Angewandte Analysis und Stochastik (WIAS)
Leibniz-Institut im Forschungsverbund Berlin e. V.
Mohrenstraße 39
10117 Berlin
Germany

Fax: +49 30 20372-303
E-Mail: preprint@wias-berlin.de
World Wide Web: http://www.wias-berlin.de/

Surface induced phase separation of a swelling hydrogel

Matthew G. Hennessy, Andreas Münch,

Barbara Wagner

Abstract

We present a formulation of the free boundary problem for a hydrogel that accounts for the interfacial free energy and finite strain due to the large deformation of the polymer network during solvent transport across the free boundary. For the geometry of an initially dry layer fixed at a rigid substrate, our model predicts a phase transition when a critical value of the solvent concentration has been reached near the free boundary. A one-dimensional case study shows that depending on the flux rate at the free boundary an initial saturation front is followed by spinodal decomposition of the hydrogel and the formation of an interfacial front that moves through the layer. Moreover, increasing the shear modulus of the elastic network delays or even suppresses phase separation.

1 Introduction

Hydrogels are, in the simplest case, two-phase systems composed of an elastic network of polymer chains immersed in a liquid solvent. The transport of solvent into and out of the network leads to the swelling and drying of the hydrogel, thereby introducing large deformations of the polymer network. Because hydrogels are omnipresent in nature, in inumerable biological processes, but also in many smart soft matter as well as medical applications, there have been many theoretical and experimental studies to understand the dynamic behaviour and pattern formation during swelling and drying processes [1, 2, 8, 10, 14, 15, 20]. The seminal work by Tanaka & Fillmore (1979) [19] argued that during swelling, a hydrogel may separate into a region of high solvent and a region of low sovent content, leading for example to a core-shell structure in swelling of an initially dry spherical hydrogel bead as well as the subsequent transient surface wrinkling instability in confined geometries T. Tanaka & Fillmore (1979) [19], [18] Sun et al. (1087), Doi [5].

The exact mechanisms explaining the dynamic processes have been subject to numerous studies during the last years, combining, as first suggested by Flory & Rehner [7], the nonlinear rubber-like elastic free energy and mixing energy that accounts for the entropy and enthalpy of mixing as due to Flory-Huggins theory developed for polymer solutions. In Drozdov et al. (2016) [6] a detailed derivation of the governing equations together with appropriate boundary conditions are given. However, they do not account for the dependence of the free energy due to the spatial gradient that develops during phase separation that leads to phases of significantly different solvent concentrations. The free energy due to the interfaces has been considered by Onuki & Puri (1999) [17] and more recently by Hong & Wang (2013) [11] including numerical simulations of pattern formation within a swelling hydrogel.

In this study we extend the derivation by Drozdov et al. (2016) [6] to include the interfacial free energy and free boundaries and derive the appropriate boundary conditions for the resulting higher order coupled system. We then formulate the problem for a thin hydrogel layer confined at a solid substrate and subject to a constant flux of solvent through the free boundary.

DOI 10.20347/WIAS.PREPRINT.2562 Berlin 2018

For the early stages of swelling we derive a reduced model equation in one dimension for the solvent concentration that is of a thin-film fourth order parabolic type with degenerate mobility. We show the existence of a saturation front and discuss different parameter regimes that impact the formation and dynamics of the front.

Our model also predicts spinodal decomposition as a critical concentration has been reached. We compare the predictions of our stability analysis for the homogeneous layer with numerical solutions of the full problem in one dimension, and we discuss the impact of non-linear elasticy on the spinodal decomposition.

2 Formulation

2.1 Bulk equations

We consider here a different derivation of a model for a swelling hydrogel, extending the procedure developed in Drozdov et al. [6] which in turn is based on Chester and Anand [3], but include the interfacial term. The term itself is chosen as the "ideal interface term" in Hong & Wang (2008) [12]; the philosophy of including it consistently in the formulation follows Gurtin's "microforce balance" approach [9]. Drozdov et al. introduce three sets of variables: Initial, which is the dry stage of the hydrogel, reference, which is the stress free state, and actual; we will adapt this scheme except that we assume that the first two states are the same.

Let C be the concentration of water molecules (number of molecules per unit volume in the initial state), and v the characteristic volume of a water molecule. The molecular incompressibility condition is

$$J = 1 + Cv. \tag{2.1}$$

Mass conservation reads

$$\dot{C} + \boldsymbol{\nabla}_0 \cdot \boldsymbol{j}_0 = 0, \tag{2.2}$$

where $\boldsymbol{j}_0$ is the flux vector in the initial state. Also satisfied is the equilibrium equation for the Cauchy stress tensor

$$\boldsymbol{\nabla} \cdot \mathbf{T} = 0. \tag{2.3}$$

The Helmholtz free energy (per unit volume in the initial configuration) is

$$\psi = \psi_1 + \psi_2 + \psi_3 + \psi_4, \tag{2.4a}$$

where the first three contributions are as in [6],

$$\psi_1 = \mu_0 C, \tag{2.4b}$$

$$\psi_2 = W(J_{e_1}, J_{e_2}, J_{e_3}), \tag{2.4c}$$

$$\psi_3 = \frac{k_B T}{v\phi_n} \left(\phi_w \ln \phi_w + \chi \phi_w \phi_n\right), \tag{2.4d}$$

where J_{e_1}, J_{e_2} and J_{e_3} are the principal invariants of the Cauchy-Green tensor for elastic deformation, χ is the Flory-Huggins parameter, and μ_0 denotes the chemical potential of a water molecule not interacting with the solid phase. The first two contribution ψ_1 and ψ_2 are the energy of water molecules not interacting with the solid phase, and the energy of the polymer network not interacting with water,

respectively, and ψ_3 is the energy of mixing of water molecules and segments of the polymer chains. The fourth contribution ψ_4 is the interfacial energy between phases. Here we use a version for an *i*deal interface as used in Hong and Wang [12], for which we give first the expression in actual coordinates and then with respect to the initial/reference state,

$$\psi_4 = \frac{\gamma}{2} J\,|\boldsymbol{\nabla} C|^2 = \frac{\gamma}{2} J H_{iK} \frac{\partial C}{\partial X_K} \frac{\partial C}{\partial X_L} H_{iL}. \tag{2.5}$$

The only difference is that we assume that the coefficient γ controlling the magnitude of the interface energy is assumed to be a constant (i.e. not depending on C).

The energy imbalance inequality. We start from the integral form of the inequality, which is [9]

$$\left\{ \int_R \psi \right\}^{\cdot} \leq - \int_{\partial R} \mu \boldsymbol{j}_0 \cdot \boldsymbol{n} + \int_{\partial R} (\boldsymbol{\xi} \cdot \boldsymbol{n}) \dot{C} + \int_{\partial R} (\mathbf{S}\boldsymbol{n} \cdot \dot{\boldsymbol{u}}). \tag{2.6}$$

The energy imbalance essentially states that the energy gain in every control volume R is at most equal to the total influx of energy and working combined. It must be satisfied for all volumes R in the initial domain of polymer. Hence, after using the divergence theorem on the right hand side, we can localise to get

$$\dot{\psi} + \boldsymbol{\nabla}_0 \cdot (\mu \boldsymbol{j}_0) - \boldsymbol{\nabla}_0 \cdot (\boldsymbol{\nabla} \xi \dot{C}) - \boldsymbol{\nabla}_0 \cdot (\mathbf{S}^T \cdot \dot{\boldsymbol{u}}) \leq 0, \tag{2.7}$$

From the incompressibility condition (2.1), we get that

$$\dot{J} - \dot{C} v = 0,$$

but also

$$\dot{J} = \frac{\partial J}{\partial \mathbf{F}} : \dot{\mathbf{F}} = J \mathbf{F}^{-T} : \dot{\mathbf{F}},$$

giving

$$\dot{C} v - J \mathbf{F}^{-T} : \dot{\mathbf{F}} = 0, \tag{2.8}$$

If we substitute (2.4) into $\dot{\psi}$ and use the constraint (2.8) times a Lagrange multiplier Π, we obtain, after using (2.2) and (2.3),

$$\begin{aligned} \left(\frac{\partial \psi}{\partial \nabla_0 C} - \boldsymbol{\xi} \right) \cdot \boldsymbol{\nabla}_0 \dot{C} + \left(\frac{\partial \psi}{\partial C} - \mu - \boldsymbol{\nabla}_0 \cdot \boldsymbol{\xi} + \Pi v \right) \dot{C} \\ + \left(\frac{\partial \psi}{\partial \mathbf{F}} - \mathbf{S} - \Pi J \boldsymbol{F}^{-T} \right) : \dot{\mathbf{F}} + \boldsymbol{\nabla}_0 \mu \cdot \boldsymbol{j}_0 \leq 0 \end{aligned} \tag{2.9}$$

The constraint (2.8) is the time derivative of the incompressibility constraint (2.1), and the multiplier Π plays the role of the osmotic pressure. The quantities $\boldsymbol{\nabla}_0 \dot{C}$, $\dot{C}$, $\dot{\mathbf{F}}$ and $\boldsymbol{\nabla}_0 \mu$ can be chosen independently at each point $\boldsymbol{X}$ and each time t. In particular, we can keep $\boldsymbol{\nabla}_0 \mu = 0$ and then vary the other three terms individually. Since none of the terms in the brackets depends on any of these three quantities, the only way to satisfy the inequality in all cases is to assume the brackets vanish identically. Hence, we obtain

$$\boldsymbol{\xi} = \frac{\partial \psi}{\partial \nabla_0 C}, \tag{2.10a}$$

$$\mu = \Pi v + \frac{\partial \psi}{\partial C} - \boldsymbol{\nabla}_0 \cdot \boldsymbol{\xi}, \tag{2.10b}$$

$$\mathbf{S} = -\Pi J \mathbf{F}^{-T} + \frac{\partial \psi}{\partial \mathbf{F}}. \tag{2.10c}$$

What remains of (2.9) is then the inequality

$$\boldsymbol{\nabla}_0\mu \cdot \boldsymbol{j}_0 \leq 0. \tag{2.11}$$

Furthermore, the Cauchy stress tensor $\boldsymbol{T}$ is related to the Piola-Kirchhoff stress tensor $\mathbf{S}$ via

$$\mathbf{T} = \frac{1}{J}\mathbf{S}\mathbf{F}^T. \tag{2.12}$$

Hence, (2.10c) becomes

$$\mathbf{T} = -\Pi\mathbf{I} + \frac{1}{J}\frac{\partial\psi}{\partial F}\mathbf{F}^T, \tag{2.13}$$

We now need to evaluate the expressions in (2.10) and (2.13) to get explicit expressions for $\mathbf{T}$ and μ. We obtain

$$\begin{aligned}\mathbf{T} = -\Pi\mathbf{I} + \frac{2}{1+Cv}\left[\frac{\partial W}{\partial J_{e_1}}\mathbf{B} - J_{e_3}\frac{\partial W}{\partial J_{e_2}}\mathbf{B}^{-1} - \left(J_{e_2}\frac{\partial W}{\partial J_{e_2}} + J_{e_3}\frac{\partial W}{J_{e_3}}\right)\mathbf{I}\right] \\ +\frac{\gamma}{2}|\boldsymbol{\nabla}C|^2\mathbf{I} - \gamma\boldsymbol{\nabla}C\otimes\boldsymbol{\nabla}C.\end{aligned} \tag{2.14}$$

The term in the last line is the Korteweg stress tensor $\boldsymbol{\sigma}^{\text{korteweg}}$ which comes from ψ_4; details of the derivation are given in appendix B. For μ, we obtain

$$\mu = \mu_0 + k_BT\left[\frac{\Pi v}{k_BT} + \ln\frac{Cv}{1+Cv} + \frac{1}{1+Cv} + \frac{\chi}{(1+Cv)^2} + \frac{\mu_{\text{grad}}}{k_BT}\right], \tag{2.15a}$$

with

$$\mu_{\text{grad}} = -\gamma\frac{\partial}{\partial X_L}\left(JH_{iL}H_{iK}\frac{\partial C}{\partial X_K}\right). \tag{2.15b}$$

Notice that for μ_{grad} we use $\mathbf{H} = \mathbf{F}^{-T}$. Notice also that the expression for μ_{grad} is given in reference coordinates, that is, the derivatives that appear there are in terms of X's. On the other hand, the other terms in (2.15a) are stated in actual coordinates.

For the purpose of calculating $\boldsymbol{j}$, it is useful to write all terms using only derivatives with respect to actual coordinates. This gives, first,

$$\begin{aligned}\mu_{\text{grad}} &= -\gamma\frac{\partial}{\partial X_L}\left(JH_{iL}H_{iK}\frac{\partial C}{\partial X_K}\right). \\ &= -\gamma\frac{\partial}{\partial X_L}\left(JH_{iL}\right)\frac{\partial C}{\partial x_i} - \gamma J\nabla^2 C,\end{aligned}$$

but

$$\frac{\partial}{\partial X_L}\left(JH_{iL}\right) = 0, \tag{2.16}$$

as we show in appendix C. Hence

$$\mu_{\text{grad}} = -\gamma J\nabla^2 C. \tag{2.17}$$

For the strain energy density W, we adopt the neoHookean expression with shear modulus G,

$$W = \frac{G}{2}\left[(J_{e_1} - 3) - \ln J_{e_3}\right]. \tag{2.18}$$

Using this in (2.14) gives

$$\mathbf{T} = -\Pi\mathbf{I} + \frac{G}{1+Cv}\left(\mathbf{B}-\mathbf{I}\right) + \gamma\left[\frac{1}{2}|\boldsymbol{\nabla}C|^2\mathbf{I} - \boldsymbol{\nabla}C\otimes\boldsymbol{\nabla}C\right]. \tag{2.19}$$

The flux in the actual configuration is

$$\boldsymbol{j} = -\frac{Dc}{k_BT}\boldsymbol{\nabla}\mu. \tag{2.20}$$

We note that in initial variables this is

$$\boldsymbol{j}_0 = -\frac{DC}{k_BT}\mathbf{F}^{-1}\mathbf{F}^{-T}\boldsymbol{\nabla}_0\mu,$$

from which we conclude that

$$\boldsymbol{\nabla}_0\mu\cdot\boldsymbol{j}_0 = -\frac{DC}{k_BT}\left|\mathbf{F}^{-T}\boldsymbol{\nabla}_0\mu\right|^2 \le 0.$$

Thus, (2.11) is satisfied.

Introducing μ into (2.20) gives

$$\boldsymbol{j} = \boldsymbol{j}_1 + \boldsymbol{j}_2 + \boldsymbol{j}_3, \tag{2.21a}$$

$$\boldsymbol{j}_1 = -D\frac{1+(1-2\chi)Cv}{(1+Cv)^4}\boldsymbol{\nabla}C, \tag{2.21b}$$

$$\boldsymbol{j}_2 = -\frac{D}{k_BT}\frac{Cv}{1+Cv}\boldsymbol{\nabla}\Pi, \tag{2.21c}$$

$$\boldsymbol{j}_3 = \frac{D\gamma}{k_BT}\frac{C}{1+Cv}\boldsymbol{\nabla}\left[(1+Cv)\nabla^2C\right] \tag{2.21d}$$

The flux vector $\boldsymbol{j}_1$ describes the transport driven by inhomogeneous water distribution and $\boldsymbol{j}_2$ describes the flux driven by the gradient of the osmotic pressure. Dropping for now $\boldsymbol{j}_3$ and taking the limit $Cv \to 0$, we get Fick's law

$$\boldsymbol{j} = -D\boldsymbol{\nabla}C; \tag{2.22}$$

conversely, in the limit $Cv \to \infty$, we get Darcy's law

$$\boldsymbol{j} = -\frac{D}{k_BT}\boldsymbol{\nabla}\Pi. \tag{2.23}$$

Darcy's law is usually written in the form

$$\boldsymbol{v}_w - \boldsymbol{v}_n = -\frac{\phi_w}{\zeta}\boldsymbol{\nabla}\Pi, \tag{2.24}$$

where $\boldsymbol{v}_w$ and $\boldsymbol{v}_n$ are velocity vectors for water and the network, and η is a coefficient of friction between water molecules and segments of chains. This friction coefficient is experimentally measured to be governed by the law, see e.g. references in Drozdov et al.

$$\zeta = \zeta_0\phi_n^\beta\phi_w^2, \qquad \beta = 1.5. \tag{2.25}$$

If in Darcy's limit we identify $\boldsymbol{j}$ with $c(\boldsymbol{v}_w - \boldsymbol{v}_n)$, the comparison gives an expression for D via

$$\frac{D}{k_BT} = \frac{c}{\zeta_0\phi_n^\beta\phi_w}, \tag{2.26}$$

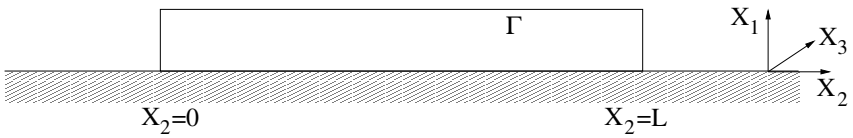

Figure 1: Schematic of the cross-section of a laterally bounded gel film that is attached to a rigid substrate (shown here in the reference state).

hence

$$D = \frac{k_B T c (1+Cv)^{\beta+1}}{\zeta_0 C v} = \frac{k_B T (1+Cv)^{\beta}}{\zeta_0 v}. \tag{2.27}$$

This then gives the following expression for the flux:

$$\boldsymbol{j} = -\frac{k_B T}{\zeta_0 v}(1+Cv)^{\beta-1}\left[\frac{1+(1-2\chi)Cv}{(1+Cv)^3}\boldsymbol{\nabla} C + \frac{Cv}{k_B T}\boldsymbol{\nabla}\Pi \right. \\ \left. -\frac{\gamma C}{k_B T}\boldsymbol{\nabla}\left[(1+Cv)\nabla^2 C)\right]\right]. \tag{2.28}$$

This then has to be transformed into initial state variables (see explanations for eqn. (26) in Drozdov et al.), to be combined with mass conservation (2.2).

2.2 Boundary conditions

Where we consider a specific situation in this section, we will use as our default a swelling film attached to a rigid substrate, see the schematic in Fig. 1. The discussion of the condition at between the gel and the bath, however, is generic.

Boundary conditions at the gel/bath interface. We assume local equilibrium at the gel/bath interface Γ, effectively assuming that equilibration at the interface is fast compared to diffusion of the solvent through the network. This requires the chemical potential of the gel and the bath to be equal, so that

$$\mu^+ = \mu^- \tag{2.29}$$

across Γ. We use the convention that $+$ and $-$ superscripts denote the limit towards the interface coming from the positive and negative normal direction, where the normal $\boldsymbol{n}$ points from the gel into the bath. So $+$ refers to the limit of the quantity in the bath, and correspondingly for $-$. The expression (2.15) applies to both the bath and the gel, but simplifies considerably in the former, as the Cv is constant and large there. Using this gives

$$\mu^+ = \mu_0 + \Pi^+ v.$$

However, we also neglect the pressure in the bath. This means we essentially assume a hydrostatic situation without a body force i.e. gravity, giving constant pressure across the bath. The constant is free so we simply set it to zero, so that

$$\Pi^+ = 0. \tag{2.30}$$

Hence

$$\mu^+ = \mu_0,$$

and therefore, from (2.29),

$$\mu^- = \mu_0 \quad \text{at } \Gamma. \tag{2.31}$$

From the gel side, we need to use the full expression for μ, supplying the variables with a $-$ superscript. Introducing this inot the preceding expression gives, finally

$$\frac{\Pi^- v}{k_B T} + \ln \frac{C^- v}{1 + C^- v} + \frac{1}{1 + C^- v} + \frac{\chi}{(1 + C^- v)^2} - \frac{\gamma J}{k_B T} \nabla^2 C^- = 0 \quad \text{at } \Gamma. \tag{2.32}$$

Drozdov et al. obtain a boundary condition for the stresses. They only spell it out for the specific geometry, e.g. the attached, flat film. We attempt a generalisation. We start from continuity of stresses

$$T^+ = T^- \tag{2.33}$$

at Γ. If we neglect the stresses arising from the motion of the water in the bath, and use (2.30), we get

$$T^+ = 0, \tag{2.34}$$

hence

$$T^- = 0. \tag{2.35}$$

Using (2.19) gives

$$-\Pi^- \mathbf{I} + \frac{G}{1 + C^- v} (\mathbf{B} - \mathbf{I}) + \frac{2\gamma}{1 + C^- v} \left[\frac{1}{2} |\boldsymbol{\nabla} C^-|^2 \mathbf{I} - \boldsymbol{\nabla} C^- \otimes \boldsymbol{\nabla} C^- \right] = 0 \tag{2.36}$$

at Γ.

A further boundary condition is needed since we have higher order derivatives of C appearing in our expression for μ. For this use the condition on the $\boldsymbol{\nabla} C$ that we also use for the side walls and at the substrate

$$\boldsymbol{\nabla} C \cdot \boldsymbol{n}_\Gamma = 0, \tag{2.37}$$

but keep in mind that this may produce boundary layers in the limit $\gamma \to 0$.

Boundary conditions at the substrate. At the bottom surface, $X_1 = 0$, the film is rigidly attached to the substrate, so we have no-displacement conditions,

$$\boldsymbol{u} = 0. \tag{2.38}$$

Moreover, the flux of material vanishes, as the substrate is assumed to be impenetrable

$$\boldsymbol{j} \cdot \boldsymbol{e}_1 = 0, \tag{2.39}$$

where $\boldsymbol{e}_i$ are the canonical unit vectors. Again, we need an additional boundary condition, and we choose

$$\boldsymbol{\nabla} C \cdot \boldsymbol{e}_1 = 0. \tag{2.40}$$

We note here that this is the same boundary condition used by for the lower-order system, so we essentially avoid boundary layers for the one-dimensional swelling problem in the limit $\gamma \to 0$.

Boundary conditions at the side walls. At the side walls, $X_2 = 0,\ L$, and $X_3 = 0,\ L$ the gel cannot move sideways but may slide freely along these walls, hence we impose

$$\boldsymbol{u} \cdot \boldsymbol{e}_k = 0, \qquad \boldsymbol{e}_1 \cdot \mathbf{T} \cdot \boldsymbol{e}_k = 0, \tag{2.41}$$

at the wall $X_k = 0,\ L$, with $k = 2, 3$. Again, we assume no-flux

$$\boldsymbol{j} \cdot \boldsymbol{e}_k = 0, \tag{2.42}$$

and adopt the additional boundary condition

$$\boldsymbol{\nabla} C \cdot \boldsymbol{e}_k = 0. \tag{2.43}$$

Remark on boundary conditions used in the literature. The boundary conditions seem to be equivalent to the boundary conditions formulated for the situation of 1D swelling of an eastomeric gel by Chester and Anand [3].

In the context of Li intercalation into silicon, Meca et al. [16] used the same boundary conditions at the substrate and I believe also at the side walls. The conditions at the side walls are also the same. However, this is not the case for the conditions at Γ, where the authors impose (2.35) and (2.37) but not (2.29) or (2.31). Instead, the latter is replaced by a Butler-Vollmer or a constant flux condition. The former actually includes a parameter for the equilibrium chemical potential and for this value, the flux is suppressed.

Curatolo et al. [4] carry out a finite element simulation for a swelling gel sphere. They use different boundary conditions at Γ (because of the geometry, the other boundary conditions are absent), using for example a flux condition at the interface between gel and bath. However, later on they note that e.g. the flux is unknown and is treated as a Lagrange parameter, which is fixed by setting the value for μ at the boundary The value of μ at the boundary is set to a negative value (for the dry gel) and then quickly increased to 0 (the value of the bath) over a time scale that is short compared to the characteristic time they introduced. It seems this is an effort to include the rapid immersion of the dry sphere into the bath.

3 Spinodal decomposition in a homogeneous gel

We collect the governing equations here for convenience:

$$\mathbf{F} = \boldsymbol{\nabla}_0 \chi, \tag{3.1}$$
$$J = \det \mathbf{F}, \tag{3.2}$$
$$J = 1 + Cv. \tag{2.1}$$
$$\dot{C} + \boldsymbol{\nabla}_0 \cdot \boldsymbol{j}_0 = 0, \tag{2.2}$$
$$\boldsymbol{\nabla} \cdot \mathbf{T} = 0. \tag{2.3}$$

$$\mathbf{T} = -\Pi \mathbf{I} + \frac{G}{1+Cv}\left(\mathbf{B} - \mathbf{I}\right) + \gamma \left[\frac{1}{2}|\boldsymbol{\nabla} C|^2 \mathbf{I} - \boldsymbol{\nabla} C \otimes \boldsymbol{\nabla} C\right], \tag{2.19}$$
$$\boldsymbol{j}_0 = J\mathbf{F}^{-1}\boldsymbol{j}, \tag{3.3}$$
$$\boldsymbol{j} = -\frac{k_B T}{\zeta_0 v}(1+Cv)^{\beta-1}\left[\frac{1+(1-2\chi)Cv}{(1+Cv)^3}\boldsymbol{\nabla} C + \frac{Cv}{k_B T}\boldsymbol{\nabla}\Pi - \frac{\gamma C}{k_B T}\boldsymbol{\nabla}\left[(1+Cv)\nabla^2 C)\right]\right]. \tag{3.4}$$

3.1 One-dimensional problem

We consider the situation whereby a dry gel undergoes uniaxial deformations of the form $\mathbf{F} = \mathrm{diag}(1,1,J(Z,t))$, which implies that $\mathbf{B} = \mathrm{diag}(1,1,B)$. The governing equations in 1D are

$$\partial_t C + \partial_Z j = 0, \tag{3.5}$$
$$\partial_Z T = 0, \tag{3.6}$$

where we note that $\partial_Z = (1+Cv)\partial_z$ and $j_0 = j$, that is, the nominal and current solvent fluxes are identical. Thus we have

$$B = J^2 = (1+Cv)^2 \tag{3.7}$$
$$T_{11} = T_{22} = -\Pi + \frac{\gamma}{2}(\partial_z C)^2 \tag{3.8}$$
$$T_{33} = -\Pi + \frac{G}{1+Cv}\left((1+Cv)^2 - 1\right) - \frac{\gamma}{2}(\partial_z C)^2, \tag{3.9}$$
$$j = -\frac{k_B T}{\zeta_0 v}(1+Cv)^{\beta-1}\left[\frac{1+(1-2\chi)Cv}{(1+Cv)^3}\partial_z C + \frac{Cv}{k_B T}\partial_z \Pi - \frac{\gamma C}{k_B T}\partial_z\left[(1+Cv)\partial_{zz} C)\right]\right]. \tag{3.10}$$

We non-dimensionalise as follows

$$z = L_0 z^*, \quad t = \frac{\zeta_0 v L_0^2}{k_B T} t^*, \quad j = \frac{k_B T}{\zeta_0 v^2 L_0} j^*, \quad T = G T^*, \quad \Pi = G\Pi^*, \tag{3.11}$$

and define the non-dimensional parameters

$$\frac{1}{g} = \frac{\gamma}{v^2}\frac{1}{L_0^2}\frac{1}{G}, \quad \omega = \frac{\gamma}{v^2}\frac{v}{k_B T}\frac{1}{L_0^2}. \tag{3.12}$$

It is convenient to introduce $C^* := Cv$ as a new variable and drop all "*" in the following non-dimensional governing equations to obtain

$$T_{33} = -\Pi + \frac{(1+C)^2 - 1}{1+C} - \frac{1}{2g}(\partial_z C)^2 \tag{3.13a}$$

$$\partial_t C = -(1+C)\partial_z j, \tag{3.13b}$$

$$j = -(1+C)^{\beta-1}\left(\frac{1+(1-2\chi)C}{(1+C)^3}\partial_z C + g\omega C\partial_z \Pi - \omega C\partial_z\left[(1+C)\partial_{zz}C\right]\right) \tag{3.13c}$$

We can now integrate the vertical stress balance and use the no-traction condition at the free surface to obtain a solution for Π and thus obtain

$$\partial_t C = -(1+C)\,\partial_z j\,, \tag{3.14a}$$

$$j = -(1+C)^{\beta-1}\left\{\frac{1+(1-2\chi)C}{(1+C)^3}\partial_z C + \omega\, g\, C\,\partial_z\left[\frac{2C+C^2}{1+C}\right] - \omega\, C\,\partial_z\left[\frac{1}{2}(\partial_z C)^2 + (1+C)\partial_{zz}C\right]\right\}. \tag{3.14b}$$

3.2 Solution of the time-dependent one-dimensional problem

We now consider a transient swelling problems whereby solvent enters the free surface of the hydrogel with a non-dimensional mass flux given by Q. Thus, the boundary conditions at the free surface $z = h(t)$ is given by

$$j = -Q, \tag{3.15a}$$

$$\partial_z C = 0, \tag{3.15b}$$

where the non-dimensional flux is given by (3.14b). Due to volume conservation, the position of the free surface must satisfy

$$h(t) = \int_0^1 (1+C)\,\mathrm{d}Z. \tag{3.16}$$

By differentiating (3.16) and using (3.14a) and (3.15a), we find that $h(t) = 1 + Q\,t$.

3.2.1 Small-time dynamics

To gain insight into the transient swelling dynamics, we consider the small-time limit of the one-dimensional problem and thus assume that $t \ll 1$. To facilitate the analysis, we make a further assumption that all of the other parameters are $O(1)$ in magnitude. For $t \ll 1$, we can immediately deduce that $h(t) = 1 + O(t)$ and thus the free boundary does not move. For small times, the swelling is expected to be localised near the free surface and only a limited amount of solvent will enter the

hydrogel, i.e. $C \ll 1$ for $t \ll 1$. Thus, it is convenient to introduce a new coordinate, $\bar{z} \ll 1$, with its origin at the hydrogel surface, defined by $\bar{z} = 1 - z$. A suitable scale for C can be derived by first noting from (3.15a) that $j = O(1)$. The dominant term in the flux relation (3.14b) is $C\partial_{\bar{z}\bar{z}\bar{z}}C$ which, when used with the fact that $j = O(1)$, implies that $C = O(\bar{z}^{3/2})$. A scale for $\bar{z}$ can now be obtained by balancing both terms in the conservation equation (3.14a), which gives $\bar{z} = O(t^{2/5})$ and $C = O(t^{3/5})$. The corresponding reduced model valid for small times is

$$\partial_t C + \omega\partial_{\bar{z}}\left(C\partial_{\bar{z}\bar{z}\bar{z}}C\right) = 0, \tag{3.17a}$$

with boundary conditions at the hydrogel surface $\bar{z} = 0$ given by

$$\partial_{\bar{z}}C = 0, \tag{3.17b}$$

$$\omega C\partial_{\bar{z}\bar{z}\bar{z}}C = Q, \tag{3.17c}$$

far-field conditions

$$C \to 0, \quad \partial_{\bar{z}}C \to 0, \tag{3.17d}$$

as $\bar{z} \to \infty$, and the initial condition $C = 0$ when $t = 0$. We see that the concentration satisfies a degenerate thin-film equation with linear mobility. The solutions to such equations are known to have compact support [13] and satisfy $C(\bar{z}, t) > 0$ for $\bar{z} < \bar{z}_f(t)$ and $C(\bar{z}, t) = 0$ for $\bar{z} \geq \bar{z}_f(t)$, where $\bar{z}_f(t)$ corresponds to a saturation front that propagates from the free surface into the bulk. By integrating (3.17a), applying the boundary condition (3.17c), and assuming there is no flux of solvent through the saturation front, we find that

$$\int_0^{\bar{z}_f(t)} C\,\mathrm{d}\bar{z} = Qt, \tag{3.18}$$

which provides an additional equation that determines the position of the saturation front.

The problem for the small-time dynamics defined by (3.17)–(3.18) has a similarity solution of the form $C = Q^{4/5}\omega^{-1/5}t^{3/5}f(\eta)$ and $\bar{z}_f(t) = F\omega^{1/5}Q^{1/5}t^{2/5}$ where the similarity variable is $\eta = \bar{z}/(\omega^{1/5}Q^{1/5}t^{2/5})$. The function f satisfies the equation

$$\frac{3}{5}f(\eta) - \frac{2}{5}\eta f'(\eta) + [f(\eta)f'''(\eta)]' = 0, \tag{3.19a}$$

where $' = \mathrm{d}/\mathrm{d}\eta$, together with the boundary conditions

$$f'(0) = 0, \quad f(0)f'''(0) = 1, \quad f(F) = 0, \quad f'(F) = 0. \tag{3.19b}$$

The last of these conditions, $f'(F) = 0$, is discussed in detail by King and Bowen [13]. The integral condition

$$\int_0^F f(\eta)\,d\eta = 1 \tag{3.19c}$$

determines the position of the free boundary F. A numerical solution to (3.19) gives $F \simeq 2.2707$, $f(0) \simeq 0.8842$, and the self-similar concentration profile shown in Figure 2.

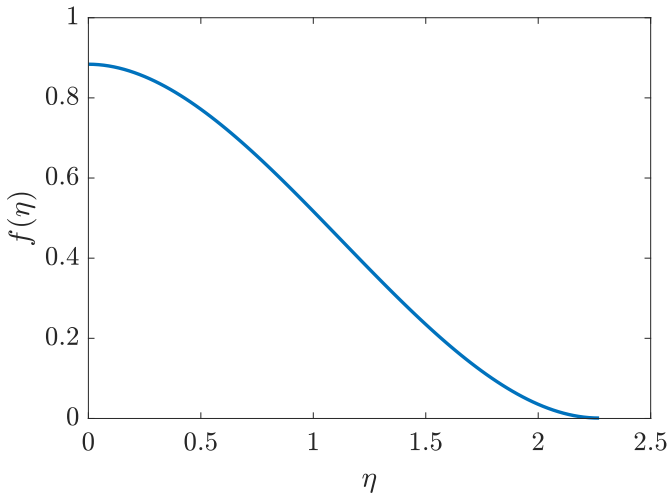

Figure 2: Numerical approximation of the small-time similarity solution of (3.19).

3.2.2 Small-time analysis for $\omega \ll 1$

Here we base the small-time limit on the fact that $\omega \ll 1$. This elucidates the fact there are multiple small-time regimes and explains why it is so hard to see the saturation front in the numerics.

When $C \ll 1$, the model reduces to

$$\partial_t C - \partial_{\bar{z}\bar{z}} C + \omega \partial_{\bar{z}} \left(C \partial_{\bar{z}\bar{z}\bar{z}} C \right) = 0, \tag{3.20}$$

with boundary conditions

$$\partial_{\bar{z}} C = 0, \tag{3.21}$$

$$\omega C \partial_{\bar{z}\bar{z}\bar{z}} C = Q, \tag{3.22}$$

at $\bar{z} = 0$.

The first time regime is captured by balancing the first and third terms in the bulk equation (3.20) and both terms in the flux BC (3.22), which gives $C \sim Q^{1/2}\omega^{-1/2}\bar{z}^{3/2}$ and $t \sim Q^{-1/2}\omega^{-1/2}\bar{z}^{5/2}$, where the length scale is undetermined. Using these concentration and time scales leads to the same problem as above, i.e. (3.17) or (3.19).

There is a second time regime which occurs when all three terms in the bulk equation and flux boundary conditions balance, which gives $t \sim Q^2\omega^2$, $z \sim Q\omega$, and $C \sim Q^2\omega$. It is interesting to know if the solution to (3.20)–(3.22) still have a sharp saturation front or whether diffusion destroys this. We note that the transition between the first and second time regime occurs when $t \sim Q^2\omega^2$, i.e. almost immediately when $\omega \ll 1$ and $Q \ll 1$.

There is also a third regime. For $Q^2\omega^2 \ll t \ll 1$ and $Q\omega \ll z \ll 1$ with $z \sim t^{1/2}$, it is only possible to balance the first and second terms in the bulk equation (3.20). Thus, we obtain a classical diffusion problem at leading order, although there should be a boundary layer near $z = 0$. The concentration profile is of the form $c(z,t) = Qt^{1/2}g(z/t^{1/2})$, where

$$g(\eta) = \eta - \eta \operatorname{erf}(\eta/2) + (2/\pi)^{1/2} \exp(-\eta^2/4). \tag{3.23}$$

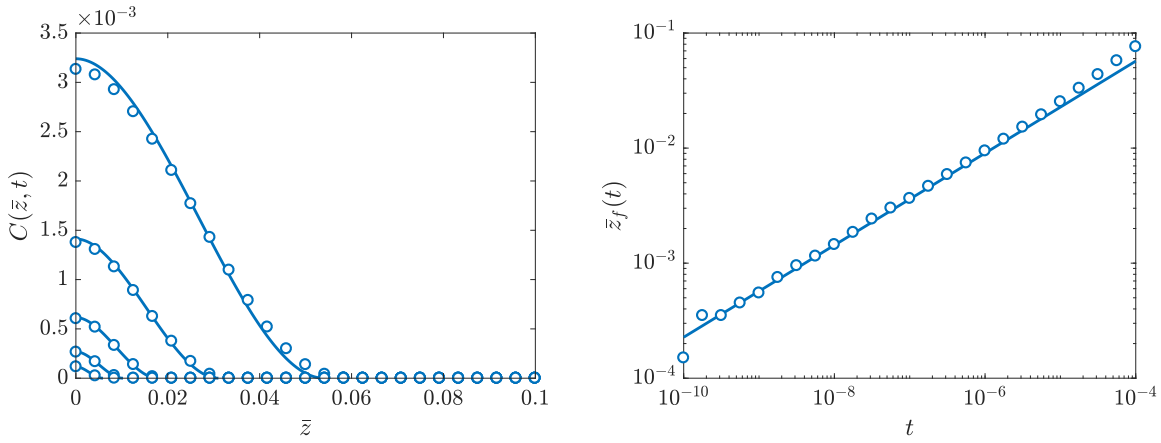

(a) (b)

Figure 3: Numerical solution of the full model (3.14) for small times showing (a) the concentration profile and (b) the position of the saturation front. The concentration profiles are shown at times $t = 3.4 \times 10^{-7}$, 1.4×10^{-6}, 5.5×10^{-6}, 2.2×10^{-5}, and 8.7×10^{-5}. Circles denote the numerical solution and lines correspond to the small-time similarity solution computed from (3.19). Parameter values are $g\omega = 0.01$, $\omega = 1$, $\chi = 1$, $\beta = 1$, and $Q = 1$.

3.2.3 Comparison with numerics

The small-time dynamics are examined by numerically solving the full one-dimensional model given by (3.14). The numerical method is based on a finite difference scheme that uses a staggered grid. The flux j_0 is solved on cell edges while the concentration C and the contribution to the chemical potential from the gradient-energy terms μ_{grad} are solved on cell midpoints. A semi-implicit method is used that treats nonlinear terms explicitly and linear terms implicitly. Thus, each time step requires the solution of a linear system of equations for C, j, and μ_{grad}. The discretised equations are formulated in terms of Lagrangian coordinates, which fixes the position of the free boundary for the hydrogel surface to $Z = 1$. The Flory–Huggins parameter is set to $\chi = 1$, the permeability exponent is taken to be $\beta = 1$, and the effective elastic constant is set to $g\omega = 0.01$. We focus on how the dynamics vary with the size of $Q\omega$.

The results of a numerical simulation with $Q = 1$ and $\omega = 1$ are shown in Figure 3 and compared with the small-time similarity solution computed from (3.19). There is excellent agreement between the numerical and asymptotic concentration profiles (Figure 3 (a)) and the position of the saturation front (Figure 3 (b)). Although the small-time analysis in Section 3.2.1 and the corresponding reduced model (3.19) are expected to be valid for $t \ll 1$, the position of the saturation front begins to deviate from the $t^{2/5}$ scaling law when $t \simeq 10^{-5}$. At this point, diffusion begins to play a role in transporting solvent across the bulk. An important implication of this deviation is that the transition to diffusion-dominated behaviour occurs quite early in the swelling process, even when all of the parameters are $O(1)$ in magnitude.

When the dimensionless flux Q and the dimensionless interface energy ω are decreased to $Q = 0.01$ and $\omega = 10^{-4}$, respectively, the small-time analysis in Section 3.2.2 predicts that the transition to diffusion-dominated behaviour occurs when $t \sim 10^{-12}$, which is essentially instantaneous. A comparison of numerical solutions with the similarity solution given by (3.23) confirms this prediction: the numerical solution is perfectly captured by the similarity solution obtained from the classical diffusion equation.

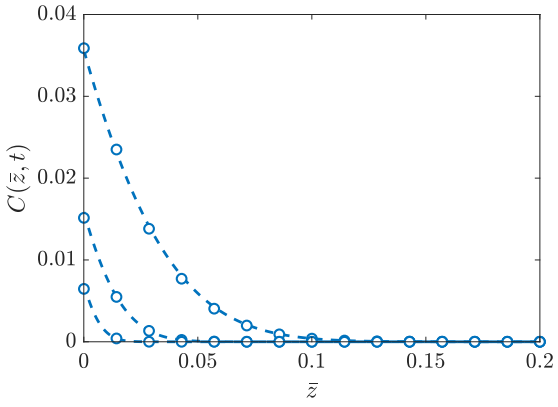

Figure 4: Numerical solution of the full model (3.14) for small times showing a concentration profile dominated by diffusion. The concentration profiles are shown at times $t = 4 \times 10^{-5}$, 2×10^{-4}, and 10^{-3}. Circles denote the numerical solution and dashed lines correspond to the small-time similarity solution given by (3.23). Parameter values are $g\omega = 0.01$, $\omega = 10^{-4}$, $\chi = 1$, $\beta = 1$, and $Q = 0.01$.

3.3 Spinodal decomposition in one dimension

Suppose now that initially we have a constant state $C = C_0$. Then a simple normal modes analysis about this state, using the ansatz

$$C = C_0 + \delta C_1 \tag{3.24}$$

yields the growth rate

$$\lambda = -(1+C_0)^\beta \left\{ \left(\frac{1+(1-2\chi)C_0}{(1+C_0)^3} + \omega\, g\, \frac{C_0((1+C_0)^2+1)}{(1+C_0)^2} \right) k^2 + \omega\, C_0(1+C_0)k^4 \right\} \tag{3.25}$$

From this we immediately see that the gel layer phase separates if

$$\frac{1+(1-2\chi)C_0}{1+C_0} + \omega\, g\, C_0 \left((1+C_0)^2+1\right) < 0 \tag{3.26}$$

is fullfilled. In particular, it shows that for $G \to \infty$ also $g \to \infty$ and hence $\chi_c \to \infty$. This means, that elasticity not only acts to suppress phase separation but for large enough shear modulus phase separation can even be excluded.

3.3.1 Numerical solution: From small-time to spinodal decomposition

Numerical simulations are used to study the onset of surface-induced phase separation and the interplay of nonlinear elasticity. In order to isolate the mechanism of phase separation, the dimensionless solvent flux is set to be $Q = 0.01$. Larger values of Q lead to the formation of solvent-rich layers near the free surface even when the thermodynamics of the system do not allow for phase separation. In this case, the formation of solvent-rich layers is due to the vastly different time scales of solvent intake and diffusive mass transport, the former of which is fast compared to the latter. For small values of the flux Q, the concentration of solvent is roughly uniform due to relatively high rate of diffusion and remains this way until spinodal decomposition occurs. In the numerical simulations, the Flory–Huggins

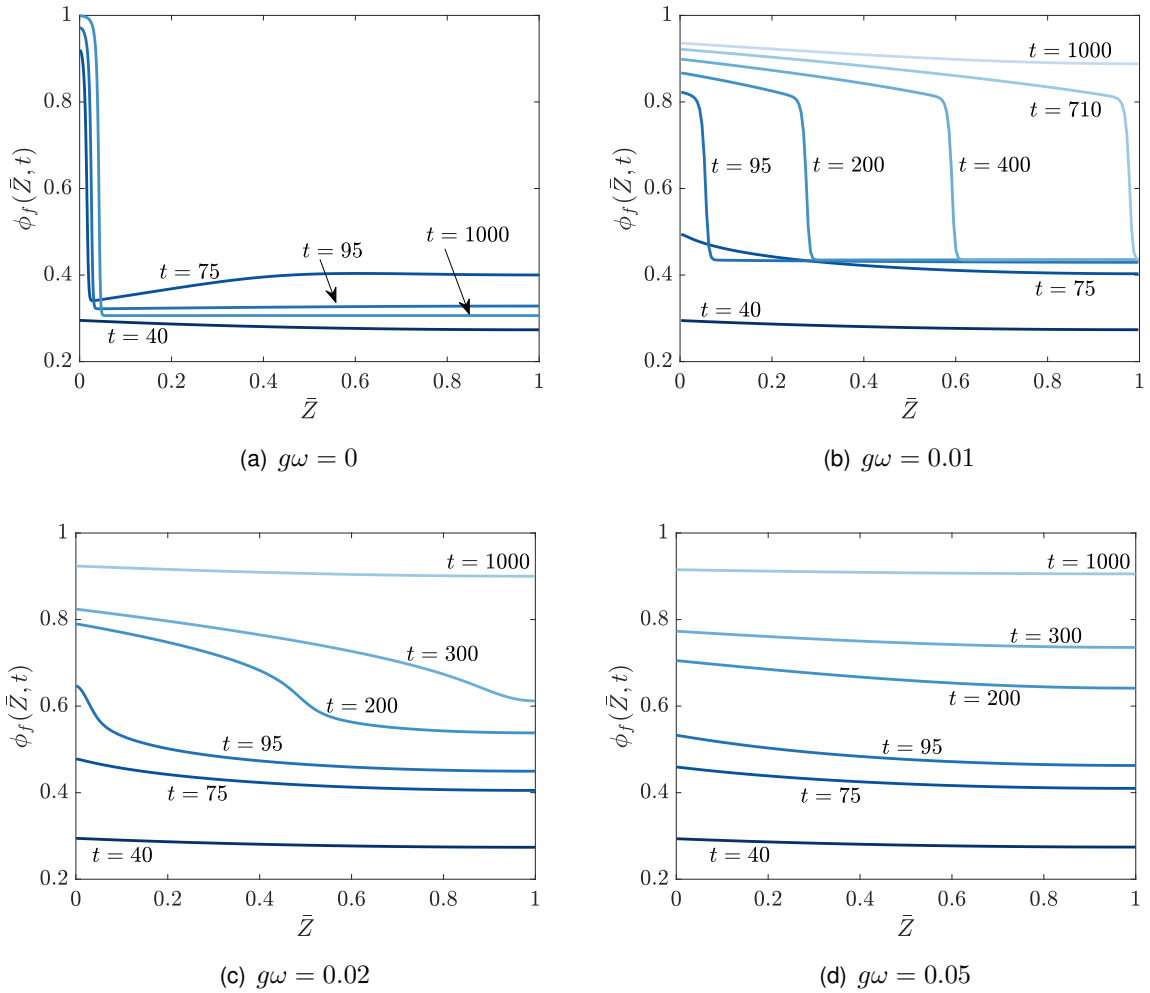

(a) $g\omega = 0$ (b) $g\omega = 0.01$

(c) $g\omega = 0.02$ (d) $g\omega = 0.05$

Figure 5: Numerical simulations of the full model (3.14) showing the onset and suppression of surface-induced phase separation for weak elasticity and strong elasticity, respectively. The parameter values are $\chi = 1$, $\omega = 10^{-6}$, $\beta = 1$, and $Q = 0.01$. For $\chi = 1$, the system has a miscibility gap when $g\omega \leq 0.019$.

parameter is set to $\chi = 1$, the permeability exponent to $\beta = 1$, and the dimensionless surface energy to $\omega = 10^{-6}$. The effective elastic constant $g\omega$ is set to 0, 0.01, 0.02, and 0.05. For this value of χ, the system exhibits a miscibility gap when $g\omega \leq 0.019$. Profiles of the solvent volume fraction $\phi_f = 1 - (1 + C)^{-1}$ are shown in Figure 5 as functions of the Lagrangian coordinate $\bar{Z} = 1 - Z$ at various times.

In the absence of elastic effects, $g\omega = 0$ (Figure 5 (a)), the system undergoes phase separation at $t \simeq 73$, forming a highly solvent-rich layer near the hydrogel surface ($\bar{Z} = 0$) and a solvent-poor layer in the bulk. The solvent-rich and solvent-poor layers are separated by a thin interfacial region centered about $\bar{Z} = \bar{S}(t)$, which propagates very slowly into the bulk. The position of the interfacial layer can be implicitly defined by the expression $\phi_f(\bar{S}(t), t) = 0.6$ and is shown as a function of time in Figure 6 (a). The finite time at which $\bar{S}$ begins to increase from zero marks the onset of phase separation. Interestingly, Figure 5 (a) shows there is a backflow of solvent from the bulk into the surface layer, which causes the surface concentration to increase at the expense of the bulk concentration. Figure 6 (b), which plots the evolution of the solvent fraction at the surface of the hydrogel and the substrate, illustrates this more clearly.

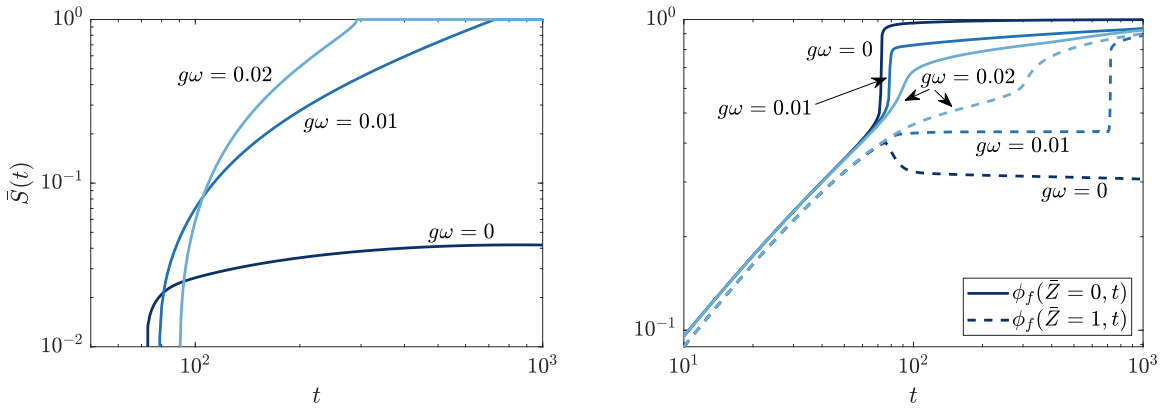

Figure 6: Evolution of the (a) position of the interfacial layer $\bar{Z} = \bar{S}(t)$ that separates solvent-rich and solvent-poor layers in the hydrogel and (b) the solvent volume fraction at the surface ($\bar{Z} = 0$) and substrate ($\bar{Z} = 1$). The position of the interfacial layer is implicitly defined by $\phi_f(\bar{S}(t), t) = 0.6$. The parameter values are $\chi = 1$, $\omega = 10^{-6}$, $\beta = 1$, and $Q = 0.01$.

When the effective elastic constant is increased to $g\omega = 0.01$ (Figure 5 (b)), the dynamics remain qualitatively similar. However, the onset of phase separation is slightly delayed and occurs at $t \simeq 79$. Furthermore, the interfacial layer separating the solvent-rich and solvent-poor layers now propagates much more rapidly into the bulk and reaches the substrate when $t \simeq 709$, which is shown in Figure 6 (a). Contrary to the inelastic case, there is no backflow of solvent. Once phase separation begins to occur, the concentration of solvent in the bulk (i.e. ahead of the solvent-rich layer) remains constant in time; see Figure 6 (b).

Increasing the effective elastic constant to $g\omega = 0.02$ prevents the system from exhibiting a miscibility gap. However, the simulation results in Figure 5 (c) indicate that the system can weakly separate into a solvent-rich and solvent-poor layer, which now occurs at $t \simeq 91$. Unlike the previous two cases, the interfacial region separating the solvent-rich and solvent-poor layers now much more diffuse. Furthermore, the solvent content ahead of the propagating layer increases in time (see Figure 6 (b)). As a result, the solvent-rich layer is able to penetrate the depth of the hydrogel and reach the substrate much faster than when $g\omega = 0$ or 0.01 (see Figure 6 (a)). When the effective elastic constant is increased to $g\omega = 0.05$ (Figure 5 (d)), the solvent concentration remains roughly uniform during the entire swelling process.

The numerical simulations show that while elasticity can delay or even suppress the onset of phase separation, it facilitates the propagation of solvent-rich layers into the bulk. The mechanism behind this enhancement is stress-assisted diffusion. The solvent-rich layer will experience a greater degree of volumetric expansion than the solvent-poor layer and hence also experience a greater elastic stress. This gradient in the elastic stress will promote the transport of solvent to the interfacial layer. As the effective elastic constant increases, this transport becomes so effective that the interfacial layer is effectively destroyed and the composition remains spatially uniform during the entire swelling process.

4 Conclusion

In this study we considered the swelling of an initially “dry” hydrogel layer fixed on a rigid susbtrate and otherwise free boundaries that allow the solvent transport into the polymer network. We derived

a model for a hydrogel that accounts for finite strain of the polymer network and higher order interfacial free energy together with the appropriate boundary conditions. For the one-dimensional case we derived reduced model equations of fourth order with degenerate mobilities that allow for similarity solutions for the saturation front that forms during the initial phase for an applied constant solvent flux. The model also predicts spinodal decomposition at a critical solvent concentration but can be delayed or even suppressed depending on the vaue of the shear modulus. Current investigations concern the corresponding problem in higher dimensions and implications on spanwise instabilities of the moving fronts.

A Glossary of Notations

We generally use Einstein's summation convention.

ψ	Helmholtz free energy (per unit volume in the initial configuration)
μ	Chemical potential of water molecules
$\boldsymbol{j}_0$	Flux vector in the initial state
$\boldsymbol{n}$	Exterior normal to the domain in question
$\boldsymbol{\xi}$	Microstress
$\boldsymbol{X}$	Initial state (=reference state) variables
$\boldsymbol{x}$	Actual coordinates, mapped from initial state coordinates via $\boldsymbol{x} = \chi(\boldsymbol{X}, t)$
$\dot{a}$	Partial time derivative $\partial_t a(\boldsymbol{X}, t)$ keeping $\boldsymbol{X}$ fixed
$\boldsymbol{u}$	Displacement, $\boldsymbol{u} = \boldsymbol{\chi}(\boldsymbol{X}, t) - \boldsymbol{x}$
$\boldsymbol{\nabla}_0$	Gradient operator in initial variables $\nabla_0 = \left(\dfrac{\partial}{\partial X_i}\right)_i$
$\boldsymbol{\nabla}$	Gradient operator in actual variables $\nabla = \left(\dfrac{\partial}{\partial x_i}\right)_i$
$\boldsymbol{v}$	Velocity $\boldsymbol{v} = \dot{\boldsymbol{\chi}}$
$\mathbf{I}$	Identity tensor
$\mathbf{A}^T$	Transpose of a tensor $\mathbf{A}$
$\mathbf{AB}$	Product of two $n \times n$ tensors, $(\mathbf{A}_{ij}\mathbf{B}_{jk})_{i,k}$
$\mathbf{A}\boldsymbol{x}$	Tensor-vector product, $(\mathbf{A}_{ij}\mathbf{x}_j)_i$
$\boldsymbol{x} \otimes \boldsymbol{y}$	tensorial vector-vector product, $\boldsymbol{x} \otimes \boldsymbol{y} = (z_{ij})_{i,j}$, with $z_{ij} = x_i y_j$
$\boldsymbol{x} \cdot \boldsymbol{y}$	inner vector-vector product, $x_i y_i$
$\mathbf{F}$	Deformation gradient tensor, $\mathbf{F} = \boldsymbol{\nabla}_0 \chi = \mathbf{I} + \boldsymbol{\nabla}_0 \boldsymbol{u}$
$\mathbf{H}$	Inverse deformation gradient tensor $\mathbf{H} = \mathbf{F}^{-T}$ (Conventions are not uniform across the literature.)
$\mathbf{B}$	Left Cauchy-Green tensors, $\mathbf{B} = \mathbf{F} \cdot \mathbf{F}^T$.
J_{e_1}	First invariant of $\mathbf{B}$: $J_{e_1} = \mathrm{tr}(\mathbf{B})$.
J_{e_2}	Second invariant of $\mathbf{B}$: $J_{e_2} = (1/2)[\mathrm{tr}(\mathbf{B})^2 - \mathrm{tr}(\mathbf{B}^2)]$.
J_{e_3}	Third invariant of $\mathbf{B}$: $J_{e_3} = \det(\mathbf{B})$.
$\mathbf{L}$	Velocity gradient, $\mathbf{L} = \dot{\mathbf{F}} \cdot \mathbf{F}^{-1}$
$\mathbf{D}$	Rate of strain tensor, $\mathbf{D} = (\mathbf{L} + \mathbf{L}^T)/2$
$\mathbf{S}$	Piola-Kirchhoff stress tensor
$\mathbf{T}$	Cauchy stress tensor
J	Determinant of the deformation gradient tensor, $J = \det \mathbf{F}$
v	Characteristic volume of a water molecule
ϕ_w	Volume fraction of water molecules, $\phi_w = Cv/(1 + Cv)$

ϕ_n Volume fraction of polymer network molecules, $\phi_n = 1/(1 + Cv)$

B Korteweg stress terms

From nonlinear solid mechanics, the nominal (first Piola–Kirchoff) stress tensor is given by

$$\mathbf{S} = \frac{\partial W}{\partial \mathbf{F}}, \tag{B.1}$$

where W is the free energy per unit of volume in the reference configuration and $\mathbf{F}$ is the deformation gradient tensor with components $\mathsf{F}_{iJ} = \partial x_i/\partial X_J$. The components of the true (Cauchy) stress tensor are given by

$$\sigma_{ij} = \frac{1}{J}\frac{\partial W}{\partial \mathsf{F}_{iK}}\mathsf{F}_{jK}, \tag{B.2}$$

where $J = \det \mathbf{F}$. The Korteweg stress can be calculated from a consideration of the interfacial free energy. This can be assumed to have the form (2.5), that is, starting from the version in current coordinates

$$\psi_4 = \frac{\gamma}{2}J|\nabla C|^2, \tag{B.3}$$

where C is the nominal concentration and ∇ is the gradient in the current configuration. Note that one can also consider $W = (\gamma/2)J|\nabla\phi_f|^2$ where ϕ_f is the current volume fraction of solvent, but the results remain unchanged.

To calculate the stress, we use the fact that

$$\frac{\partial}{\partial x_i} = \mathsf{H}_{iJ}\frac{\partial}{\partial X_J}, \tag{B.4}$$

where $\mathbf{H} = \mathbf{F}^{-T}$. Thus, the interfacial energy can be written as

$$\psi_4 = \frac{\gamma}{2}J\mathsf{H}_{aK}\mathsf{H}_{aL}\frac{\partial C}{\partial X_K}\frac{\partial C}{\partial X_L}. \tag{B.5}$$

To evaluate the derivatives of W with respect to $\mathbf{F}$, we use

$$\frac{\partial J}{\partial \mathsf{F}_{iK}} = J\mathsf{H}_{iK}, \quad \frac{\partial \mathsf{H}_{aB}}{\partial \mathsf{F}_{iK}} = -\mathsf{H}_{aK}\mathsf{H}_{iB}. \tag{B.6}$$

It is simpler to first calculate the Korteweg stress in the current configuration (i.e., in terms of the Cauchy stress). Using $\mathsf{H}_{aB}\mathsf{F}_{bB} = \delta_{ab}$ and

$$\frac{\partial}{\partial \mathsf{F}_{iJ}}\left(\mathsf{H}_{aK}\mathsf{H}_{aL}\right)\mathsf{F}_{lJ} = -\mathsf{H}_{iK}\mathsf{H}_{lL} - \mathsf{H}_{iL}\mathsf{H}_{lK}, \tag{B.7}$$

it can be shown that

$$\frac{\partial}{\partial \mathsf{F}_{iJ}}\left(\mathsf{H}_{aK}\mathsf{H}_{aL}\frac{\partial C}{\partial X_K}\frac{\partial C}{\partial X_L}\right)\mathsf{F}_{lJ} = -2\frac{\partial C}{\partial x_i}\frac{\partial C}{\partial x_l} \tag{B.8}$$

When combining everything, we see that

$$\sigma_{ij}^{\text{korteweg}} = \frac{\gamma}{2}\frac{\partial C}{\partial x_k}\frac{\partial C}{\partial x_k}\delta_{ij} - \gamma\frac{\partial C}{\partial x_i}\frac{\partial C}{\partial x_j}. \tag{B.9}$$

In tensor form, this is equivalent to

$$\boldsymbol{\sigma}^{\text{korteweg}} = \frac{\gamma}{2}|\nabla C|^2\mathbf{I} - \gamma\nabla C \otimes \nabla C, \tag{B.10}$$

where $\mathbf{I}$ is the identity tensor. This is the last term in $\mathbf{T}$ in (2.14).

C Transformation of the interface terms

To evaluate the contribution to the chemical potential from the interfacial energy, we need to evaluate

$$\frac{\partial}{\partial X_L}\left(J\mathsf{H}_{aL}\right) = \frac{\partial J}{\partial X_L}\mathsf{H}_{aL} + J\frac{\partial \mathsf{H}_{aL}}{\partial X_L} \tag{C.1}$$

Using the identities (6) in the Korteweg notes, we find that

$$\frac{\partial}{\partial X_L}\left(J\mathsf{H}_{aL}\right) = J\left(\mathsf{H}_{iK}\mathsf{H}_{aL}\frac{\partial \mathsf{F}_{iK}}{\partial X_L} - \mathsf{H}_{aQ}\mathsf{H}_{pL}\frac{\partial \mathsf{F}_{pQ}}{\partial X_L}\right). \tag{C.2}$$

Now we can use the equality of mixed second derivatives to write

$$\frac{\partial \mathsf{F}_{pQ}}{\partial X_L} = \frac{\partial}{\partial X_L}\left(\frac{\partial x_p}{\partial X_Q}\right) = \frac{\partial}{\partial X_Q}\left(\frac{\partial x_p}{\partial X_L}\right) = \frac{\partial \mathsf{F}_{pL}}{\partial X_Q}. \tag{C.3}$$

This gives

$$\frac{\partial}{\partial X_L}\left(J\mathsf{H}_{aL}\right) = J\left(\mathsf{H}_{iK}\mathsf{H}_{aL}\frac{\partial \mathsf{F}_{iK}}{\partial X_L} - \mathsf{H}_{pL}\mathsf{H}_{aQ}\frac{\partial \mathsf{F}_{pL}}{\partial X_Q}\right) = 0, \tag{C.4}$$

as claimed in (2.16).

References

[1] T. Bertrand, J. Peixinho, S. Mukhopadhyay, and C. W. MacMinn. Dynamics of swelling and drying in a spherical gel. *Physical Review Applied*, 6(6), 2016. doi: 10.1103/PhysRevApplied.6.064010.

[2] S. Cai and Z. Suo. Equations of state for ideal elastomeric gels. *EPL (Europhysics Letters)*, 97 (3):34009, 2012. doi: 10.1209/0295-5075/97/34009.

[3] S. A. Chester and L. Anand. A coupled theory of fluid permeation and large deformations for elastomeric materials. *Journal of the Mechanics and Physics of Solids*, 58(11):1879–1906, 2010. doi: 10.1016/j.jmps.2010.07.020.

[4] M. Curatolo, P. Nardinocchi, E. Puntel, and L. Teresi. Transient instabilities in the swelling dynamics of a hydrogel sphere. *Journal of Applied Physics*, 122(14):145109, 2017. doi: 10.1063/1.5007229.

[5] M. Doi. Gel dynamics. volume 325, pages 796–798. 1987.

[6] A. D. Drozdov, A. A. Papadimitriou, J. H. M. Liely, and C. G. Sanporean. Constitutive equations for the kinetics of swelling of hydrogels. *Mechanics of Materials*, 102:61–73, 2016. doi: 10.1016/j.mechmat.2016.08.012.

[7] P. J. Flory and J. Rehner. Statistical Mechanics of Cross-Linked Polymer Networks I. Rubberlike Elasticity. *The Journal of Chemical Physics*, 11(11):512–520, 1943. doi: http://dx.doi.org/10.1063/1.1723791.

[8] T. Gan, Y. Guan, and Y. Zhang. Thermogelable PNIPAM microgel dispersion as 3D cell scaffold: Effect of syneresis. *Journal of Materials Chemistry*, 20(28):5937, 2010. doi: 10.1039/c0jm00338g.

[9] M. E. Gurtin. Generalized Ginzburg-Landau and Cahn-Hilliard equations based on a microforce balance. *Physica D: Nonlinear Phenomena*, 92(3):178–192, 1996. doi: 10.1016/0167-2789(95)00173-5.

[10] M. G. Hennessy, A. Vitale, O. K. Matar, and J. T. Cabral. Monomer diffusion into static and evolving polymer networks during frontal photopolymerisation. *Soft Matter*, 13(48):9199–9210, 2017. doi: 10.1039/C7SM01279A.

[11] W. Hong and X. Wang. A phase-field model for systems with coupled large deformation and mass transport. *Journal of the Mechanics and Physics of Solids*, 61(6):1281–1294, 2013.

[12] W. Hong, X. Zhao, J. Zhou, and Z. Suo. A theory of coupled diffusion and large deformation in polymeric gels. *Journal of the Mechanics and Physics of Solids*, 56(5):1779–1793, 2008. doi: 10.1016/j.jmps.2007.11.010.

[13] J. R. King and M. Bowen. Moving boundary problems and non-uniqueness for the thin film equation. *European Journal of Applied Mathematics*, 12(3):321âĂŞ356, 2001. doi: 10.1017/S0956792501004405.

[14] J. Krawczyk, S. Croce, T. C. B. McLeish, and B. Chakrabarti. Elasticity dominated surface segregation of small molecules in polymer mixtures. *Physical Review Letters*, 116(20), 2016. doi: 10.1103/PhysRevLett.116.208301.

[15] C. W. MacMinn, E. R. Dufresne, and J. S. Wettlaufer. Large Deformations of a Soft Porous Material. *Physical Review Applied*, 5(4):044020, 2016. doi: 10.1103/PhysRevApplied.5.044020.

[16] E. Meca, A. Münch, and B. Wagner. Sharp-interface formation during lithium intercalation into silicon. *European Journal of Applied Mathematics*, 29(1):118–145, 2018. doi: 10.1017/S0956792517000067.

[17] A. Onuki and S. Puri. Spinodal decomposition in gels. *Physical Review E*, 59(2):R1331–R1334, 1999. doi: 10.1103/PhysRevE.59.R1331.

[18] S.-T. Sun, Y. Hirokawa, S. Katayama, J. Kucera, Y. Hirose, and T. Amiya. Mechanical instability of gels at the phase transition. *Nature*, 325:796–798, 1987.

[19] T. Tanaka and D. J. Fillmore. Kinetics of swelling of gels. *The Journal of Chemical Physics*, 70(3):1214–1218, 1979. doi: 10.1063/1.437602.

[20] J. Yoon, S. Cai, Z. Suo, and R. C. Hayward. Poroelastic swelling kinetics of thin hydrogel layers: Comparison of theory and experiment. *Soft Matter*, 6(23):6004, 2010. doi: 10.1039/c0sm00434k.